

Elastic Diffusion Transformer

Jiangshan Wang^{1,2} Zeqiang Lai^{2,3} Jiarui Chen^{2,4} Jiayi Guo¹ Hang Guo¹
 Xiu Li¹ Xiangyu Yue³ Chuncho Guo²

Abstract

Diffusion Transformers (DiT) have demonstrated remarkable generative capabilities but remain highly computationally expensive. Previous acceleration methods, such as pruning and distillation, typically rely on a fixed computational capacity, leading to insufficient acceleration and degraded generation quality. To address this limitation, we propose **Elastic Diffusion Transformer (E-DiT)**, an adaptive acceleration framework for DiT that effectively improves efficiency while maintaining generation quality. Specifically, we observe that the generative process of DiT exhibits substantial sparsity (i.e., some computations can be skipped with minimal impact on quality), and this sparsity varies significantly across samples. Motivated by this observation, E-DiT equips each DiT block with a lightweight router that dynamically identifies sample-dependent sparsity from the input latent. Each router adaptively determines whether the corresponding block can be skipped. If the block is not skipped, the router then predicts the optimal MLP width reduction ratio within the block. During inference, we further introduce a block-level feature caching mechanism that leverages router predictions to eliminate redundant computations in a training-free manner. Extensive experiments across 2D image (Qwen-Image and FLUX) and 3D asset (Hunyuan3D-3.0) demonstrate the effectiveness of E-DiT, achieving up to $\sim 2\times$ speedup with negligible loss in generation quality. Code will be available at <https://github.com/wangjiangshan0725/Elastic-DiT>.

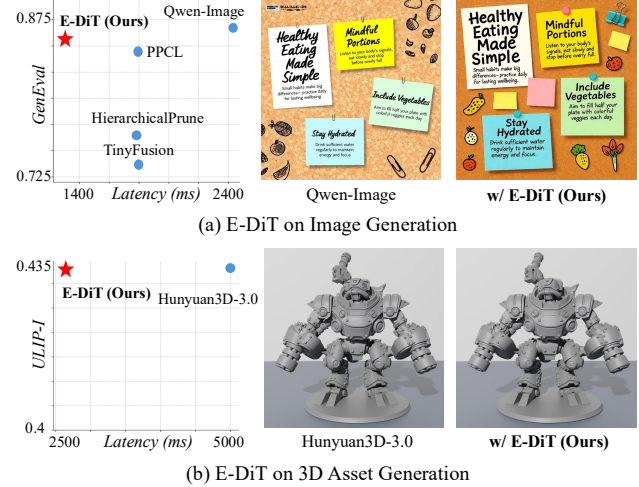


Figure 1. Performance of Elastic Diffusion Transformer (E-DiT) across diverse generation foundation models and modalities.

1. Introduction

Diffusion models have achieved remarkable progress in recent years, demonstrating strong performance across diverse modalities, including images (Labs, 2024; Wu et al., 2025; Esser et al., 2024), videos (Yang et al., 2024; Wang et al., 2025), and 3D assets (Lai et al., 2025a;d; Zhao et al., 2025). Despite these successes, they usually suffer from substantial computational overhead due to the large model sizes, which significantly limit their practical deployment. As a result, improving the efficiency of diffusion models while maintaining high generation quality has become a critical and challenging research problem.

A common strategy for accelerating diffusion models is to reduce the computational cost through pruning or distillation (Daniel Verdú, 2024; Ma et al., 2025; Kwon et al., 2025). These methods typically adopt a static design, where a fixed, smaller model architecture is uniformly applied across all denoising steps and input conditions. However, such static strategies overlook the fact that different modules within the generation process contribute unequally to the final output (Wimbauer et al., 2024; Liu et al., 2025; Zhao et al., 2024), resulting in a suboptimal trade-off between efficiency and generation quality. To mitigate this issue, several recent works explore dynamic network structures for accelerating

¹Tsinghua University ²Tencent Hunyuan ³MMLab, CUHK ⁴HITSZ. Correspondence to: Zeqiang Lai <laizeqiang@outlook.com>, Xiangyu Yue <xyyue@ie.cuhk.edu.hk>, Chuncho Guo <chunchaoguo@tencent.com>.

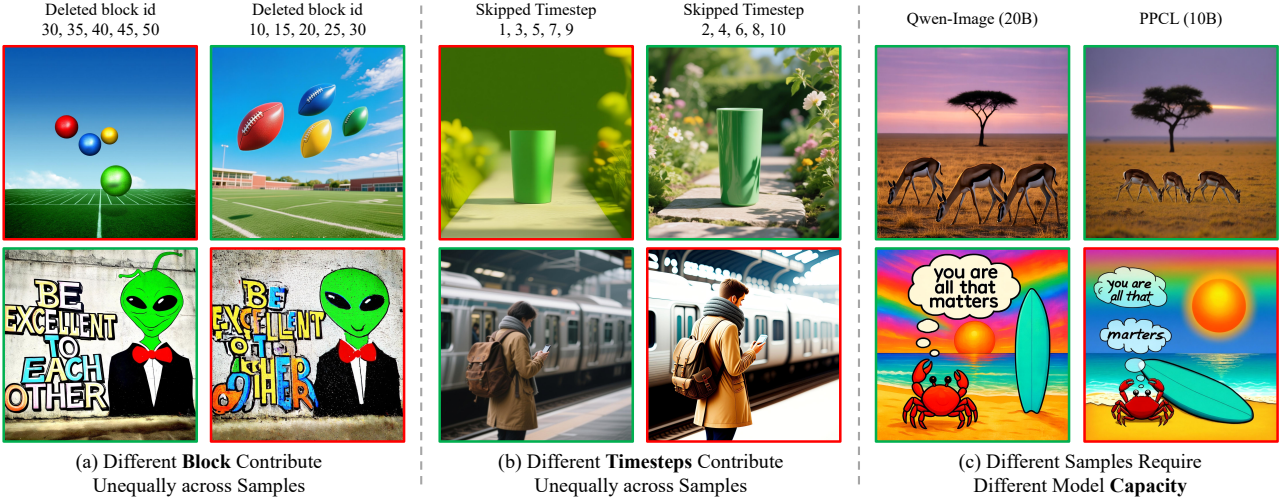


Figure 2. Sample-dependent sparsity in the generation process. We use Qwen-Image (Wu et al., 2025) to illustrate our observations.(a) Images generated after removing different subsets of DiT blocks from Qwen-Image, showing that block importance varies across samples. (b) Results obtained by skipping selected denoising timesteps using a timestep-wise feature caching strategy (Liu et al., 2025), demonstrating content-dependent sensitivity to timestep removal. (c) Comparison between images generated by the Qwen-Image base model (20B) and a pruned variant (10B) (Ma et al., 2025), highlighting that computational requirements vary with sample difficulty.

DiT models. Nevertheless, they often suffer from limited flexibility, such as requiring non-trivial architectural modifications when adapting to different backbones (Zhao et al., 2024) or activating a fixed number of parameters regardless of input complexity (Zheng et al., 2025b).

In this work, we aim to develop a general acceleration framework for diverse DiT backbones that can adaptively allocate computation according to the generated content. Specifically, we observe that the generation process exhibits significant sparsity: certain computations during denoising contribute only marginally to the final generation quality. Importantly, this sparsity is content-dependent rather than uniform across samples, as evidenced by three key aspects (Figure 2). First, different DiT blocks contribute unequally across samples (Figure 2a). Skipping a particular subset of blocks may have negligible impacts on the generation quality of some samples while severely degrading others, and different block subsets affect different samples. Second, denoising timesteps also exhibit uneven importance across samples (Figure 2b). The effect of skipping timesteps varies with the input content, similar to the behavior observed when skipping blocks. Third, computational demand correlates with the complexity of the generated samples (Figure 2c). While a lightweight model is enough to generate high-quality results for relatively easy samples, more complex samples require additional computation to maintain generation fidelity.

To exploit the sample-dependent sparsity in the diffusion generation process, we propose **Elastic Diffusion Transformer (E-DiT)**, a general and adaptive acceleration framework for diffusion transformers. E-DiT accelerates gener-

ation in a sample-adaptive manner through three complementary components: (1) adaptive block skipping, which dynamically skips entire transformer blocks whose contributions to generation are predicted to be marginal; (2) adaptive MLP width reduction, which adjusts the activated MLP width within non-skipped blocks according to sample complexity; and (3) block-wise caching, which further eliminates redundant computation by reusing intermediate features across adjacent denoising steps in a training-free manner. Concretely, each transformer block in E-DiT is equipped with a lightweight router conditioned on the input latent and the denoising timestep. The router predicts whether the block can be skipped, and for blocks that remain active, it further determines the effective MLP width within the block. During training, we jointly optimize a performance loss to preserve generation quality and an efficiency loss to encourage efficient routing decisions. Notably, we observe that the learned router predictions naturally capture the relative importance of different blocks. Leveraging this property, we further introduce a block-wise caching mechanism that uses router predictions as a criterion for feature reusing across denoising steps, enabling additional inference acceleration without extra training.

We evaluate E-DiT across multiple modalities, including Qwen-Image (Wu et al., 2025) and FLUX (Labs, 2024) for image generation, as well as Hunyuan3D-3.0 (Team, 2025) for 3D asset generation. Experimental results demonstrate that E-DiT substantially reduces inference cost with negligible degradation in quality, while being broadly applicable and compatible with various DiT backbones.

2. Related Work

2.1. Diffusion Model

Diffusion models (Ho et al., 2020; Song et al., 2020a;b; Rombach et al., 2022; Liu et al., 2022) have emerged as a prominent paradigm for high-fidelity generation, which generate the sample through denoising from a standard Gaussian noise. In recent years, diffusion transformers (DiTs) (Peebles & Xie, 2023) have shown strong scalability and have become the mainstream architecture of modern large-scale foundation models across modalities, represented by FLUX (Labs, 2024) and Qwen-Image (Wu et al., 2025) for the image generation; HunyuanVideo (Kong et al., 2024), CogVideoX (Yang et al., 2024), and Wan2.1 (Wang et al., 2025) for video generation; Hunyuan3D (Lai et al., 2025a; Zhao et al., 2025), LATTICE (Lai et al., 2025b), and Trellis (Xiang et al., 2024) for 3D asset generation.

2.2. Diffusion Model Acceleration

High-quality generation usually requires dozens of denoising steps and expensive transformer computations at each step, resulting in substantial inference latency and compute cost. To mitigate this issue, prior works have explored acceleration via step distillation (Cheng et al., 2025; Lu & Song, 2024; Zheng et al., 2025a; Geng et al., 2025a; Lu et al., 2022; Song et al., 2023; Lai et al., 2025c), model architecture compression (Ma et al., 2025; Kwon et al., 2025; Daniel Verdú, 2024; Fang et al., 2025), and training-free methods such as sparse attention (Zhang et al., 2025; Xi et al., 2025), token merging (Bolya et al., 2022; Wang et al., 2024a) and feature caching (Selvaraju et al., 2024; Wimbauer et al., 2024; Kahatapitiya et al., 2024; Guo et al., 2026). However, these methods usually adopt fixed network structures and parameters for all samples, ignoring sample-specific variability, which could lead to a less favorable quality-efficiency trade-off.

2.3. Dynamic Neural Networks

Dynamic neural networks (Han et al., 2021) adapt computation to individual inputs by conditionally activating different parts of the network to reduce redundancy. Representative works include conditional computation with dynamic depth or width, as well as token- or head-level sparsification in Transformers (Meng et al., 2022; Song et al., 2021; Wang et al., 2024c; Rao et al., 2021; Liang et al., 2022; Li et al., 2021). Recent efforts have recently explored dynamic mechanisms in diffusion transformers, including converting dense backbones into Mixture-of-Experts structures (Zheng et al., 2025b; Cheng et al.; Wei et al., 2025; Shi et al., 2025) and dynamically selecting attention heads and tokens (Zhao et al., 2024). However, these methods often exhibit limited flexibility, such as fixed expert grouping or activation patterns,

and require non-trivial structural redesign when applied to different backbones or modalities.

3. Method

In this section, we present the design of Elastic Diffusion Transformer (E-DiT) in detail. We first introduce the model architecture of E-DiT, including the router design and adaptive mechanisms for block skipping and MLP width reduction. Next, we describe the training strategy based on a joint quality–efficiency objective. Finally, we present the inference process of E-DiT, where block-wise caching is employed to further accelerate generation by exploiting temporal redundancy across denoising steps.

3.1. Preliminaries

Rectified Flow (Liu et al., 2022) formulates generative modeling as learning a linear transport path between the data distribution π_0 and a noise distribution π_1 via an ordinary differential equation (ODE):

$$d\mathbf{x}_t = v(\mathbf{x}_t, t) dt, \quad t \in [0, 1], \quad (1)$$

where the velocity field v is parameterized by a network ϵ_θ . Given $\mathbf{x}_0 \sim \pi_0$ and $\mathbf{x}_1 \sim \pi_1$, the trajectory is defined as $\mathbf{x}_t = (1 - t)\mathbf{x}_0 + t\mathbf{x}_1$, yielding the training objective

$$\min_{\theta} \mathbb{E}_{t \sim \mathcal{U}(0,1)} \left[\|(\mathbf{x}_1 - \mathbf{x}_0) - \epsilon_\theta(\mathbf{x}_t, t)\|^2 \right]. \quad (2)$$

During inference, samples are generated by numerically solving the learned ODE from Gaussian noise (Lu et al., 2022; Wang et al., 2024b), using a solver such as Euler. Compared to DDPM (Ho et al., 2020), Rectified Flow achieves high-quality generation with substantially fewer sampling steps, making it particularly suitable for large-scale generative models (Wu et al., 2025; Labs, 2024; Lai et al., 2025a).

Multi-Modal Diffusion Transformer (DiT) (Peebles & Xie, 2023) demonstrates the scalability and effectiveness of Transformer architectures for diffusion-based generative modeling. Extending this framework, MMDiT (Labs, 2024; Wu et al., 2025) integrates conditioning information via self-attention applied jointly to both data and condition tokens. An MMDiT model comprises a stack of Transformer blocks, each consisting of a joint multi-head self-attention (MHSA) module over data and condition tokens, followed by a multi-layer perceptron (MLP). The MLP consists of two linear layers with an intermediate non-linear activation. Specifically, given the input $\mathbf{z} \in \mathbb{R}^{L \times D}$, where L is the sequence length and D is the feature dimension, the standard MLP first projects \mathbf{z} to a higher-dimension H , applies a non-linear activation (e.g., GELU), and then projects it back to the original dimension D , i.e.,

$$\text{MLP}(\mathbf{z}) = \sigma(\mathbf{z}\mathbf{W}_1)\mathbf{W}_2, \quad (3)$$

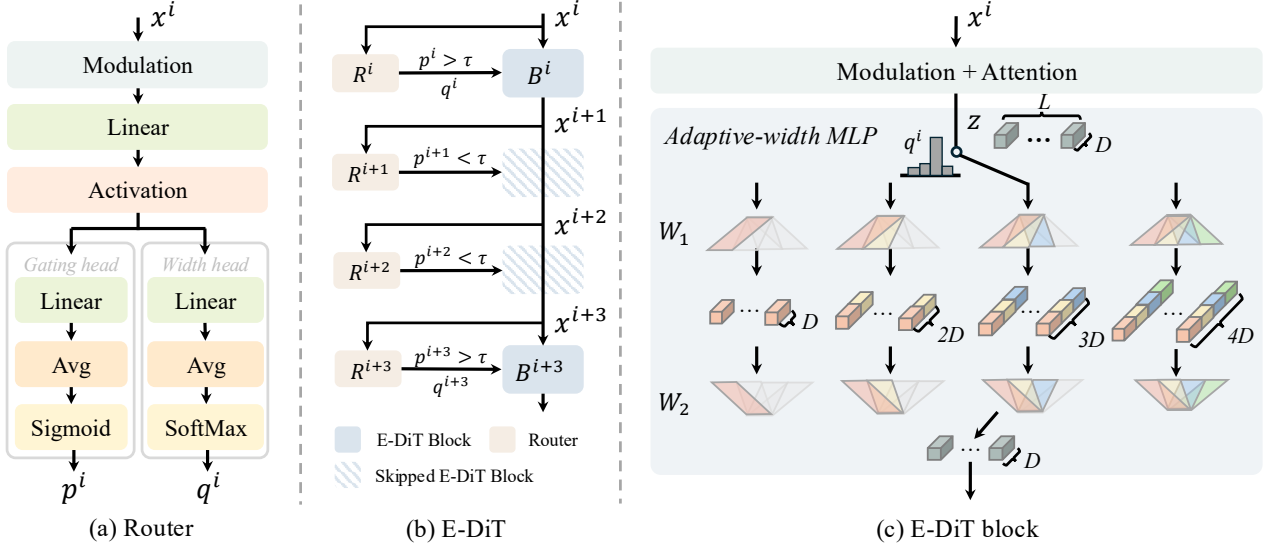


Figure 3. Overall pipeline of Elastic Diffusion Transformer (E-DiT). (a). The architecture of the router, which predicts p_g and p_w , indicating whether the block can be skipped and the width of the MLP within the block, respectively. (b). The overall structure of the E-DiT, where each transformer block is equipped with a router. (c). The structure of the transformer block within the E-DiT, where the width of the MLP is adaptively reduced according to the router’s prediction.

where $\mathbf{W}_1 \in \mathbb{R}^{D \times H}$ and $\mathbf{W}_2 \in \mathbb{R}^{H \times D}$ are linear projections and $\sigma(\cdot)$ is the activation function. We refer to the ratio H/D as the width of the MLP, which is typically set to 4 in most generation models.

3.2. Model Designs

Router Architecture. Given a Diffusion Transformer (DiT) with n blocks $\{\mathbf{B}^i\}_{i=1}^n$, we equip each block \mathbf{B}^i with a lightweight router \mathbf{R}^i to enable adaptive computation. For a given input, \mathbf{R}^i first predicts whether the block should be activated; if activated, it further predicts the appropriate MLP width within that block.

Formally, let $\mathbf{x}_t^i \in \mathbb{R}^{L \times D}$ denote the input latent to block \mathbf{B}^i at diffusion step t . Within the router, we first apply timestep-conditioned modulation using Layer Normalization (LN) followed by element-wise scaling and shifting:

$$\tilde{\mathbf{x}}_t^i = (1 + \gamma(t)) \odot \text{LN}(\mathbf{x}_t^i) + \delta(t), \quad (4)$$

where $\gamma(t), \delta(t) \in \mathbb{R}^D$ are timestep-dependent scale and shift parameters obtained via a linear projection of the timestep embedding $\mathbf{E}(t) \in \mathbb{R}^D$, and \odot denotes element-wise multiplication. The modulated features $\tilde{\mathbf{x}}_t^i$ are then projected and passed through a non-linear activation:

$$\mathbf{h} = \sigma(\tilde{\mathbf{x}}_t^i \mathbf{W}) \in \mathbb{R}^{L \times H_r}. \quad (5)$$

where $\mathbf{W} \in \mathbb{R}^{D \times H_r}$ and $H_r \ll D$ to keep the router lightweight and efficient.

Based on \mathbf{h} , the router produces two outputs via separate linear heads and global averaging, i.e., (1). A gating logit

ℓ_t^i for adaptive block skipping. (2) A width logit vector $\mathbf{u}_t^i \in \mathbb{R}^4$ for adaptive MLP width reduction.

$$\ell_t^i = \frac{1}{L} \sum_{j=1}^L \mathbf{h}[j, :] \mathbf{W}_g, \quad \mathbf{u}_t^i = \frac{1}{L} \sum_{j=1}^L \mathbf{h}[j, :] \mathbf{W}_w, \quad (6)$$

where $\mathbf{W}_g \in \mathbb{R}^{H_r \times 1}$ and $\mathbf{W}_w \in \mathbb{R}^{H_r \times 4}$ denote the parameters of the gating and width heads, respectively.

Adaptive Block Skipping. Given the scalar logit $\ell_t^i \in \mathbb{R}$ predicted by the router, we convert it to a probability via the sigmoid function: $p_t^i = \sigma(\ell_t^i) \in [0, 1]$. The corresponding block \mathbf{B}^i is skipped if p_t^i falls below a predefined threshold τ (set to 0.5 in our experiments), allowing the model to eliminate redundant computation.

During training, the discrete block-skipping operation is non-differentiable. To address this, we adopt the Straight-Through Estimator (STE) (Bengio et al., 2013), which allows gradients to propagate through the gating decisions. Specifically, we define the gate variable as:

$$g_t^i = \mathbb{1}[p_t^i \geq \tau] + p_t^i - \text{StopGrad}(p_t^i), \quad (7)$$

where $\mathbb{1}[\cdot]$ is the indicator function, returning 1 if the input is true and 0 otherwise. The output for the i th block is then computed as:

$$\mathbf{x}_t^{i+1} = \mathbf{x}_t^i + g_t^i \cdot (\mathbf{B}^i(\mathbf{x}_t^i) - \mathbf{x}_t^i), \quad (8)$$

To encourage computational efficiency, we regularize the routing by constraining the average gate probability $\bar{p} = \frac{1}{n} \sum_{i=1}^n p_t^i$ to match a target $\rho_g \in (0, 1)$ via the gating loss:

$$\mathcal{L}_{\text{gating}} = (\bar{p} - \rho_g)^2. \quad (9)$$

During inference, we directly skipped the blocks with $p_t^i < \tau$ to achieve acceleration, i.e.,

$$\mathbf{x}_t^{i+1} = \begin{cases} \mathbf{x}_t^i, & p_t^i < \tau, \\ \mathbf{B}^i(\mathbf{x}_t^i), & p_t^i \geq \tau. \end{cases} \quad (10)$$

Adaptive MLP Width Reduction. For blocks that are not skipped, we further reduce computation by dynamically adjusting the MLP width from the original $H/D = 4$ according to a set of predefined reduction ratios $\mathcal{S} = \{\frac{1}{4}, \frac{1}{2}, \frac{3}{4}, 1\}$. Specifically, given the router prediction $\mathbf{u}_t^i \in \mathbb{R}^4$, we first compute width probabilities via softmax:

$$\mathbf{q}_t^i = \text{softmax}(\mathbf{u}_t^i) \in \mathbb{R}^4. \quad (11)$$

The width with the highest probability is then selected:

$$k = \text{argmax}_j \mathbf{q}_t^i[j], \quad \hat{s}_t^i = \mathcal{S}[k]. \quad (12)$$

During training, we implement the adaptive MLP by masking intermediate activations to preserve differentiability:

$$\text{MLP}_{\text{adapt}}(\mathbf{z}) = \left(\sigma(\mathbf{z}\mathbf{W}_1) \odot \mathbf{m}(\hat{s}_t^i) \right) \mathbf{W}_2, \quad (13)$$

where \odot denotes element-wise multiplication and $\mathbf{m}(\hat{s}_t^i) \in \{1, 0\}^H$ represents a mask which only keeps the first $\hat{s}_t^i \cdot H$ part of the feature along the hidden dimension.

To encourage more efficient width selection, we regularize the averaged MLP width across all non-skipped blocks. Formally, the average width reduction for the block \mathbf{B}^i at the timestep t is defined as $r_t^i = \sum_{j=1}^4 \mathbf{q}_t^i[j] s[j]$. Since width allocation is only meaningful when the block is not skipped, we mask out skipped blocks through $\mathbb{1}[p_t^i \geq \tau]$. The masked global average width reduction is computed as

$$\bar{r} = \frac{\sum_{i=1}^n \mathbb{1}[p_t^i \geq \tau] r_t^i}{\sum_{i=1}^n \mathbb{1}[p_t^i \geq \tau]}. \quad (14)$$

We encourage \bar{r} to match a target width budget $\rho_w \in (0, 1)$ via $\mathcal{L}_{\text{width}}$:

$$\mathcal{L}_{\text{width}} = (\bar{r} - \rho_w)^2. \quad (15)$$

During inference, the adaptive MLP width is implemented by explicit matrix slicing to avoid computation on deactivated channels:

$$\text{MLP}_{\hat{s}_t^i}(\mathbf{z}) = \sigma(\mathbf{z}\widetilde{\mathbf{W}}_1)\widetilde{\mathbf{W}}_2, \quad (16)$$

where $\widetilde{\mathbf{W}}_1 = \mathbf{W}_1[:, :H \cdot \hat{s}_t^i]$, $\widetilde{\mathbf{W}}_2 = \mathbf{W}_2[:, :H \cdot \hat{s}_t^i, :]$, yielding actual acceleration by skipping computation on the deactivated channels.

3.3. Training and Inference

Training Pipeline. We train E-DiT end-to-end on top of a pretrained diffusion Transformer. At the start of training, all routers are set to be fully open, i.e., each block is activated with full MLP width, ensuring that training begins from the original dense model behavior and avoiding unstable

Algorithm 1 Pseudo-Code for E-DiT Inference

Input:

$\mathbf{x}_T \sim \mathcal{N}(\mathbf{0}, \mathbf{I})$	Initial Gaussian Noise
T	Number of denoising steps
$\{\mathbf{B}^i\}_{i=1}^N$	Network blocks
$\{\mathbf{R}^i\}_{i=1}^N$	Routers
$\{\mathcal{C}^i \leftarrow \emptyset\}_{i=1}^N$	Feature bank
τ	Block skipping threshold
δ	Borderline margin
K	Maximum reuse limit

Denoising Process:

for $t = T, T-1, \dots, 0$ do	
$\mathbf{x}_t^1 \leftarrow \mathbf{x}_t$	
for $i = 1, 2, \dots, N$ do	
$p_t^i, \mathbf{q}_t^i \leftarrow \mathbf{R}^i(\mathbf{x}_t^i, t)$	
if $p_t^i < \tau$ then	
$\mathbf{x}_t^{i+1} \leftarrow \mathbf{x}_t^i$	Directly skip the block
continue	
end if	
if $\tau \leq p_t^i \leq \tau + \delta$ and $\mathcal{C}^i \neq \emptyset$ and $k^i < K$ then	
$\mathbf{x}_t^{i+1} \leftarrow \mathbf{x}_t^i + \Delta^i$ Skip the block through feature reusing	
$k^i \leftarrow k^i + 1$	
continue	
end if	
$\mathbf{x}_t^{i+1} \leftarrow \mathbf{B}^i(\mathbf{x}_t^i, \mathbf{q}_t^i)$ Inference with adaptive MLP width	
$\Delta^i \leftarrow \mathbf{x}_t^{i+1} - \mathbf{x}_t^i$ Cache the residual	
$k^i \leftarrow 0$ Reset reuse counter	
$\mathcal{C}^i \leftarrow (\Delta^i, k^i)$	
end for	
$\mathbf{x}_{t-1} \leftarrow \text{DENOISESTEP}(\mathbf{x}_t^{N+1}, t)$ Update latent	
end for	
Output: \mathbf{x}_0	Final denoised sample

early-stage optimization. During training, given a mini-batch of latent inputs and randomly sampled timesteps, each router predicts the block gate probability p_t^i and the width distribution \mathbf{q}_t^i for each block \mathbf{B}_i (Sec. 3.2). The overall training objective combines quality and efficiency:

$$\mathcal{L} = \mathcal{L}_{\text{perf}} + \lambda \mathcal{L}_{\text{eff}}, \quad (17)$$

where λ balances the two terms (we set $\lambda = 1$ in experiments). The performance loss $\mathcal{L}_{\text{perf}}$ is the flow-matching objective in Equation (2), used by the underlying diffusion backbone, while the efficiency regularization $\mathcal{L}_{\text{eff}} = \mathcal{L}_{\text{gating}} + \mathcal{L}_{\text{width}}$ encourages sample- and timestep-adaptive routing and width allocation. This formulation allows E-DiT to learn dynamic, content-dependent computation while preserving the generation quality of the original dense model.

Inference Pipeline & Block-wise Caching. During inference, E-DiT dynamically adapts both block execution and MLP widths. For each block \mathbf{B}^i , the router predicts a gating probability $p_t^i \in [0, 1]$ and a width distribution $\mathbf{q}_t^i \in \mathbb{R}^4$ (Sec. 3.2) at each denoising step t . A block is skipped when $p_t^i < \tau$ (we set $\tau = 0.5$); otherwise, it is activated with the selected MLP width.

While adaptive block skipping and MLP width reduction al-

ready eliminate most redundant computation with minimal quality loss, we observe that some active blocks ($p_t^i \geq \tau$) have gating probabilities close to the threshold, suggesting further potential for acceleration. To exploit this, we define a borderline region $p_t^i \in [\tau, \tau + \delta]$, where blocks are not directly skipped but likely contribute marginally. For such blocks, we leverage temporal redundancy across denoising steps via a block-wise caching mechanism, reusing intermediate features to further reduce computation.

Specifically, at timestep t , when the \mathbf{B}^i is activated, we compute its residual update as

$$\Delta^i = \mathbf{B}^i(\mathbf{x}_t^i, \mathbf{q}_t^i) - \mathbf{x}_t^i, \quad (18)$$

and store it in a feature bank \mathcal{C}^i . At a later timestep \tilde{t} , if the gating probability $p_{\tilde{t}}^i$ of this block falls within the borderline region $[\tau, \tau + \delta]$ and a cached residual in \mathcal{C}^i is available, we skip the full block computation and update the latent via

$$\mathbf{x}_{\tilde{t}}^{i+1} = \mathbf{x}_{\tilde{t}}^i + \Delta^i. \quad (19)$$

Otherwise, a full forward pass is performed, and the feature bank is refreshed with the newly computed residual. To prevent error accumulation, each cached residual is reused at most K times before recomputation.

Unlike prior caching methods that require designing complicated criteria to determine when to reuse features, E-DiT naturally leverages the router prediction p_t^i as a principled cache indicator, providing a simple yet effective mechanism to further reduce redundant computation. Overall, the inference process of E-DiT is illustrated in Algorithm 1.

4. Experiments

4.1. Experimental Setup

Implementation Details. We implement E-DiT on several representative foundation models for generative modeling across both 2D image and 3D asset modalities, including Qwen-Image (Wu et al., 2025), FLUX (Labs, 2024), and Hunyuan3D-3.0 (Team, 2025). For Qwen-Image, we train two versions of our E-DiT, termed *E-DiT-base* and *E-DiT-turbo*. Specifically, E-DiT-base adopts $\rho_g = 0.6$ for adaptive block skipping, $\rho_w = 0.65$ for adaptive MLP width reduction, and block-wise caching with $\delta = 0.1$ and $K = 5$. E-DiT-turbo applies more aggressive acceleration, with $\rho_g = 0.5$, $\rho_w = 0.6$, $\delta = 0.15$, and $K = 10$. For FLUX, we set $\rho_g = 0.5$, $\rho_w = 0.6$, and use block-wise caching with $\delta = 0.1$ and $K = 3$. For Hunyuan3D-3.0, we use $\rho_g = 0.45$, $\rho_w = 0.5$, $\delta = 0.15$, and $K = 5$. The number of denoising steps T is set to 30, 28, and 5 for Qwen-Image, FLUX, and Hunyuan3D-3.0, respectively, following their default configurations. Following previous work (Cheng et al., 2025; Chen et al., 2025c; Geng et al., 2025b), we train image generation models on the BLIP3o-60K (Chen et al., 2025b) and ShareGPT-4o (Chen et al.,

Table 1. Quantitative results for text-to-image generation on Qwen-Image. L. denotes inference latency (milliseconds).

Methods	L.↓	DPG↑	GenEval↑	T2I-CompBench↑		
				B-VQA	UniDet	S-CoT
Base model	2431	88.9	0.870	0.709	0.532	82.47
TinyFusion	1789	80.7	0.739	0.689	0.464	78.99
HP	1786	83.3	0.766	0.706	0.487	79.94
PPCL	1792	87.9	0.847	0.750	0.524	82.15
E-DiT-base	1702	88.1	0.893	0.719	0.536	82.34
E-DiT-turbo	1283	85.4	0.853	0.711	0.519	81.68

Table 2. Quantitative results for text-to-image generation on FLUX.1-dev. L. denotes inference latency (milliseconds).

Methods	L.↓	DPG↑	GenEval↑	T2I-CompBench↑		
				B-VQA	UniDet	S-CoT
Base model	715	83.8	0.665	0.640	0.426	78.57
Dense2MoE	513	76.2	0.475	0.494	0.340	77.50
DyDiT	423	80.3	0.676	-	-	-
TinyFusion	534	77.2	0.511	0.584	0.369	74.17
HP	543	75.7	0.503	0.579	0.371	74.99
PPCL	535	80.0	0.605	0.615	0.391	78.15
E-DiT	374	80.5	0.671	0.612	0.402	77.91

2025a) datasets, totaling approximately 100K images. For 3D asset generation, we use the internal dataset. All experiments of training are conducted on 32 NVIDIA H20 GPUs. Inference is conducted on a single NVIDIA H20 GPU.

Baselines. For image generation, we compare E-DiT against several state-of-the-art pruning-based acceleration methods, including FLUX.1 Lite (Daniel Verdú, 2024), TinyFusion (Fang et al., 2025), HierarchicalPrune (HP) (Kwon et al., 2025), and PPCL (Ma et al., 2025). We additionally include dynamic acceleration methods, namely Dense2MoE (Zheng et al., 2025b) and DyDiT (Zhao et al., 2024). For PPCL and DyDiT, we directly report the results from their original papers, while results for the remaining baselines are taken from the PPCL benchmark. For visual comparison, we compare our methods with open-source baselines. The prompts for visual comparison are provided in the Appendix. For 3D asset generation, we compare E-DiT with the unaccelerated Hunyuan3D-3.0 baseline. More information about baselines is provided in the Appendix.

Evaluation Metrics. For image generation, we report results on DPG-Bench (Hu et al., 2024), GenEval (Ghosh et al., 2023), and T2I-CompBench (Huang et al., 2025). For 3D asset generation, performance is evaluated using ULIP (Xue et al., 2023) and Uni3D (Zhou et al., 2023) scores, together with qualitative comparisons. Inference efficiency is measured by the per-step latency on a single H20 GPU for both the baseline methods and E-DiT. We also provide visual comparisons between E-DiT and baselines to illustrate the effectiveness of our method.



Figure 4. Visual comparisons between E-DiT-turbo and open-source baselines based on Qwen-Image.

Table 3. Quantitative results of shape generation methods.

Methods	ULIP-I \uparrow	Uni3D-I \uparrow	Latency (ms) \downarrow
Hunyuan3D-3.0	0.1446	0.4334	5012
E-DiT	0.1473	0.4332	2587

Table 5. Ablation study of different initialization strategies.

Initialization Strategy	DPG \uparrow	GenEval \uparrow
Random init	78.6	0.801
Full-capacity init	85.4	0.853

Table 4. Ablation study of different acceleration components.

Skip Block	Reduced Width	Block Cache	L. \downarrow	DPG \uparrow	GenEval \uparrow
<i>non-adaptive</i>					
✓	—	—	1514	83.7	0.843
✓	✓	—	1967	87.6	0.895
✓	✓	✓	1643	85.8	0.857
			1283	85.4	0.853

4.2. Text-to-Image Generation

We evaluate E-DiT on Qwen-Image and FLUX, with quantitative results respectively reported in Table 1 and Table 2. On both models, E-DiT can achieve roughly 2 \times speedup over the base architectures while maintaining consistent performance across benchmarks. We note that DyDiT achieves similar quality metrics on FLUX compared with E-DiT, but our method achieves lower latency. Moreover, E-DiT and DyDiT are not exclusive and could be combined to achieve further acceleration. Visual comparisons in Figure 4 further demonstrate that the accelerated models preserve the ability to synthesize complex visual content, including accurate long-text rendering and coherent spatial compositions.

4.3. Image-to-3D Generation

For 3D asset generation, we implement E-DiT on Hunyuan3D-3.0 and compare model performance before and after acceleration. For quantitative evaluation, we report ULIP-I (Xue et al., 2023) and Uni3D-I (Zhou et al., 2023) scores, which measure the similarity between the generated meshes and the input images (Table 3). The results show that E-DiT achieves nearly a 2 \times speedup while maintaining comparable generation quality. Visual comparisons (Figure 5) also demonstrate that the accelerated model preserves the ability to generate high-fidelity geometric details.

4.4. Discussions

Ablation of E-DiT Components. We systematically evaluate the contribution of each E-DiT component (Table 5). Both adaptive block skipping and MLP width reduction individually provide notable acceleration. Building on these, block-wise caching further enhances the efficiency, achieving the lowest latency with negligible quality degradation. To assess the importance of adaptive computing, we also train a non-adaptive baseline that applies random block removal and width reduction prior to training, calibrated to match the latency of our adaptive model. Despite comparable latency, this static model shows substantially worse



Figure 5. Visual comparison of Hunyan3D 3.0 without and with E-DiT



Figure 6. Ablation study of block-wise caching.

generation quality, highlighting that adaptive computing is essential for achieving an effective trade-off between efficiency and quality.

Ablation of Block-wise Caching. We analyze the effectiveness of block-wise caching and the impact of its hyperparameters (Figure 6). First, we observe that directly skipping those borderline blocks results in a noticeable degradation in generation quality. In addition, the acceleration achieved by direct skipping differs from that of block-wise caching, although the threshold is set to be the same (e.g., $\delta = 0.015$ in Figure 6), as the two strategies induce different latent

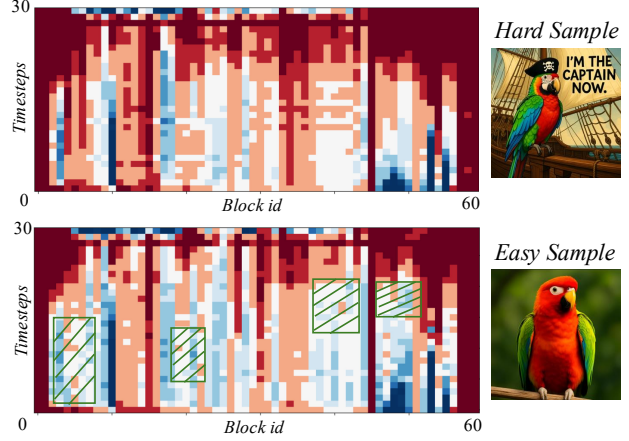


Figure 7. Visualization of the router predictions.

representations, leading to different router predictions in subsequent steps and blocks. Increasing the maximum reuse count K of cached features has only a marginal effect on generation quality and shows diminishing benefits for latency reduction beyond a certain point. In contrast, the cache activation threshold δ plays a more critical role: a larger δ results in caching a greater fraction of blocks, substantially degrading generation quality.

Ablation of Initialization. We initialize the router to preserve the full model capacity, i.e., no blocks are skipped, and all MLPs operate at their full width at the beginning of training. We find that this initialization significantly im-

proves training stability and consistently leads to better final performance. This suggests that gradually learning adaptive acceleration from a full-capacity starting point is crucial for effective optimization.

Analysis of Router Behavior. We visualize router predictions across denoising timesteps in Figure 7. Red points indicate gating probabilities above 0.5, while blue points denote probabilities below 0.5; lighter red points correspond to values near the threshold, likely to be handled by block-wise caching. The visualization reveals that certain DiT blocks (e.g., the first two and the last three blocks) are consistently critical to generation quality and are rarely skipped. Furthermore, E-DiT demonstrates input-dependent behavior: for simpler inputs, such as images with clear layouts and blurred backgrounds, routers assign lower probabilities to more blocks, enabling more aggressive skipping and faster inference. In contrast, more complex inputs with intricate backgrounds or text trigger higher probabilities across more blocks, reflecting the need for increased computation to preserve generation quality.

5. Conclusion

In this work, we propose Elastic Diffusion Transformer (E-DiT), a general adaptive framework for efficient diffusion generation. In E-DiT, each DiT block is equipped with a router that dynamically predicts whether the block can be skipped. For non-skipped blocks, the router further determines the appropriate MLP width. During inference, we introduce a block-wise caching mechanism that leverages router predictions to reduce temporal redundancy across denoising steps. Extensive experiments on both image and 3D asset generation demonstrate the effectiveness of E-DiT, achieving roughly 2 \times acceleration on Qwen-Image, FLUX, and Hunyuan3D-3.0 with negligible quality degradation.

Impact Statement

This paper presents work whose goal is to advance the field of machine learning. There are many potential societal consequences of our work, none of which we feel must be specifically highlighted here.

References

Bengio, Y., Léonard, N., and Courville, A. Estimating or propagating gradients through stochastic neurons for conditional computation. In *arXiv preprint arXiv:1308.3432*, 2013.

Bolya, D., Fu, C.-Y., Dai, X., Zhang, P., Feichtenhofer, C., and Hoffman, J. Token merging: Your vit but faster. *arXiv preprint arXiv:2210.09461*, 2022.

Chen, J., Cai, Z., Chen, P., Chen, S., Ji, K., Wang, X., Yang, Y., and Wang, B. Sharegpt-4o-image: Aligning multimodal models with gpt-4o-level image generation. *arXiv preprint arXiv:2506.18095*, 2025a.

Chen, J., Xu, Z., Pan, X., Hu, Y., Qin, C., Goldstein, T., Huang, L., Zhou, T., Xie, S., Savarese, S., et al. Blip3-o: A family of fully open unified multimodal models-architecture, training and dataset. *arXiv preprint arXiv:2505.09568*, 2025b.

Chen, J., Xue, L., Xu, Z., Pan, X., Yang, S., Qin, C., Yan, A., Zhou, H., Chen, Z., Huang, L., et al. Blip3o-next: Next frontier of native image generation. *arXiv preprint arXiv:2510.15857*, 2025c.

Cheng, K., He, X., Yu, L., Tu, Z., Zhu, M., Wang, N., Gao, X., and Hu, J. Diff-moe: Diffusion transformer with time-aware and space-adaptive experts. In *Forty-second International Conference on Machine Learning*.

Cheng, Z., Sun, P., Li, J., and Lin, T. Twinflow: Realizing one-step generation on large models with self-adversarial flows. *arXiv preprint arXiv:2512.05150*, 2025.

Daniel Verdú, J. M. Flux.1 lite: Distilling flux1.dev for efficient text-to-image generation. 2024.

Esser, P., Kulal, S., Blattmann, A., Entezari, R., Müller, J., Saini, H., Levi, Y., Lorenz, D., Sauer, A., Boesel, F., et al. Scaling rectified flow transformers for high-resolution image synthesis. In *Forty-first international conference on machine learning*, 2024.

Fang, G., Li, K., Ma, X., and Wang, X. Tinyfusion: Diffusion transformers learned shallow. In *Proceedings of the Computer Vision and Pattern Recognition Conference*, pp. 18144–18154, 2025.

Geng, Z., Deng, M., Bai, X., Kolter, J. Z., and He, K. Mean flows for one-step generative modeling. *arXiv preprint arXiv:2505.13447*, 2025a.

Geng, Z., Wang, Y., Ma, Y., Li, C., Rao, Y., Gu, S., Zhong, Z., Lu, Q., Hu, H., Zhang, X., et al. X-omni: Reinforcement learning makes discrete autoregressive image generative models great again. *arXiv preprint arXiv:2507.22058*, 2025b.

Ghosh, D., Hajishirzi, H., and Schmidt, L. Geneval: An object-focused framework for evaluating text-to-image alignment. *Advances in Neural Information Processing Systems*, 36:52132–52152, 2023.

Guo, H., Jia, Z., Li, J., Li, B., Cai, Y., Wang, J., Li, Y., and Lu, Y. Efficient autoregressive video diffusion with dummy head. *arXiv preprint arXiv:2601.20499*, 2026.

Han, Y., Huang, G., Song, S., Yang, L., Wang, H., and Wang, Y. Dynamic neural networks: A survey. *IEEE Transactions on Pattern Analysis and Machine Intelligence*, 44(11):7436–7456, 2021.

Ho, J., Jain, A., and Abbeel, P. Denoising diffusion probabilistic models. *Advances in neural information processing systems*, 33:6840–6851, 2020.

Hu, X., Wang, R., Fang, Y., Fu, B., Cheng, P., and Yu, G. Ella: Equip diffusion models with lilm for enhanced semantic alignment, 2024. URL <https://arxiv.org/abs/2403.05135>.

Huang, K., Duan, C., Sun, K., Xie, E., Li, Z., and Liu, X. T2i-compbench++: An enhanced and comprehensive benchmark for compositional text-to-image generation. *IEEE Transactions on Pattern Analysis and Machine Intelligence*, 2025.

Kahatapitiya, K., Liu, H., He, S., Liu, D., Jia, M., Zhang, C., Ryoo, M. S., and Xie, T. Adaptive caching for faster video generation with diffusion transformers. *arXiv preprint arXiv:2411.02397*, 2024.

Kong, W., Tian, Q., Zhang, Z., Min, R., Dai, Z., Zhou, J., Xiong, J., Li, X., Wu, B., Zhang, J., et al. Hunyuan-video: A systematic framework for large video generative models. *arXiv preprint arXiv:2412.03603*, 2024.

Kwon, Y. D., Li, R., Li, S., Li, D., Bhattacharya, S., and Venieris, S. I. Hierarchicalprune: Position-aware compression for large-scale diffusion models. *arXiv preprint arXiv:2508.04663*, 2025.

Labs, B. F. Flux. <https://github.com/black-forest-labs/flux>, 2024.

Lai, Z., Zhao, Y., Liu, H., Zhao, Z., Lin, Q., Shi, H., Yang, X., Yang, M., Yang, S., Feng, Y., et al. Hunyuan3d 2.5: Towards high-fidelity 3d assets generation with ultimate details. *arXiv preprint arXiv:2506.16504*, 2025a.

Lai, Z., Zhao, Y., Zhao, Z., Liu, H., Lin, Q., Huang, J., Guo, C., and Yue, X. Lattice: Democratize high-fidelity 3d generation at scale. *arXiv preprint arXiv:2512.03052*, 2025b.

Lai, Z., Zhao, Y., Zhao, Z., Liu, H., Wang, F., Shi, H., Yang, X., Lin, Q., Huang, J., Liu, Y., et al. Unleashing vecset diffusion model for fast shape generation. *arXiv preprint arXiv:2503.16302*, 2025c.

Lai, Z., Zhao, Y., Zhao, Z., Yang, X., Huang, X., Huang, J., Yue, X., and Guo, C. Natex: Seamless texture generation as latent color diffusion. *arXiv preprint arXiv:2511.16317*, 2025d.

Langley, P. Crafting papers on machine learning. In Langley, P. (ed.), *Proceedings of the 17th International Conference on Machine Learning (ICML 2000)*, pp. 1207–1216, Stanford, CA, 2000. Morgan Kaufmann.

Li, C., Wang, G., Wang, B., Liang, X., Li, Z., and Chang, X. Dynamic slimmable network. In *Proceedings of the IEEE/CVF Conference on computer vision and pattern recognition*, pp. 8607–8617, 2021.

Liang, Y., Ge, C., Tong, Z., Song, Y., Wang, J., and Xie, P. Not all patches are what you need: Expediting vision transformers via token reorganizations. *arXiv preprint arXiv:2202.07800*, 2022.

Liu, F., Zhang, S., Wang, X., Wei, Y., Qiu, H., Zhao, Y., Zhang, Y., Ye, Q., and Wan, F. Timestep embedding tells: It’s time to cache for video diffusion model. In *Proceedings of the Computer Vision and Pattern Recognition Conference*, pp. 7353–7363, 2025.

Liu, X., Gong, C., and Liu, Q. Flow straight and fast: Learning to generate and transfer data with rectified flow. *arXiv preprint arXiv:2209.03003*, 2022.

Lu, C. and Song, Y. Simplifying, stabilizing and scaling continuous-time consistency models. *arXiv preprint arXiv:2410.11081*, 2024.

Lu, C., Zhou, Y., Bao, F., Chen, J., Li, C., and Zhu, J. Dpm-solver++: Fast solver for guided sampling of diffusion probabilistic models. *arXiv preprint arXiv:2211.01095*, 2022.

Ma, J., Peng, Q., Zhu, X., Xie, P., Chen, C., and Lu, H. Pluggable pruning with contiguous layer distillation for diffusion transformers. *arXiv preprint arXiv:2511.16156*, 2025.

Meng, L., Li, H., Chen, B.-C., Lan, S., Wu, Z., Jiang, Y.-G., and Lim, S.-N. Adavit: Adaptive vision transformers for efficient image recognition. In *CVPR*, pp. 12309–12318, 2022.

Peebles, W. and Xie, S. Scalable diffusion models with transformers. In *Proceedings of the IEEE/CVF International Conference on Computer Vision*, pp. 4195–4205, 2023.

Rao, Y., Zhao, W., Liu, B., Lu, J., Zhou, J., and Hsieh, C.-J. Dynamiccvit: Efficient vision transformers with dynamic token sparsification. *Advances in neural information processing systems*, 34:13937–13949, 2021.

Rombach, R., Blattmann, A., Lorenz, D., Esser, P., and Ommer, B. High-resolution image synthesis with latent diffusion models. In *Proceedings of the IEEE/CVF conference on computer vision and pattern recognition*, pp. 10684–10695, 2022.

Selvaraju, P., Ding, T., Chen, T., Zharkov, I., and Liang, L. Fora: Fast-forward caching in diffusion transformer acceleration. *arXiv preprint arXiv:2407.01425*, 2024.

Shi, M., Yuan, Z., Yang, H., Wang, X., Zheng, M., Tao, X., Zhao, W., Zheng, W., Zhou, J., Lu, J., et al. Diffmoe: Dynamic token selection for scalable diffusion transformers. *arXiv preprint arXiv:2503.14487*, 2025.

Song, J., Meng, C., and Ermon, S. Denoising diffusion implicit models. *arXiv preprint arXiv:2010.02502*, 2020a.

Song, L., Zhang, S., Liu, S., Li, Z., He, X., Sun, H., Sun, J., and Zheng, N. Dynamic grained encoder for vision transformers. *Advances in Neural Information Processing Systems*, 34:5770–5783, 2021.

Song, Y., Sohl-Dickstein, J., Kingma, D. P., Kumar, A., Ermon, S., and Poole, B. Score-based generative modeling through stochastic differential equations. *arXiv preprint arXiv:2011.13456*, 2020b.

Song, Y., Dhariwal, P., Chen, M., and Sutskever, I. Consistency models. *arXiv preprint arXiv:2303.01469*, 2023.

Team, H. Hunyuan3d-3.0. <https://3d.hunyuanglobal.com/>, 2025.

Wang, A., Ai, B., Wen, B., Mao, C., Xie, C.-W., Chen, D., Yu, F., Zhao, H., Yang, J., Zeng, J., Wang, J., Zhang, J., Zhou, J., Wang, J., Chen, J., Zhu, K., Zhao, K., Yan, K., Huang, L., Feng, M., Zhang, N., Li, P., Wu, P., Chu, R., Feng, R., Zhang, S., Sun, S., Fang, T., Wang, T., Gui, T., Weng, T., Shen, T., Lin, W., Wang, W., Wang, W., Zhou, W., Wang, W., Shen, W., Yu, W., Shi, X., Huang, X., Xu, X., Kou, Y., Lv, Y., Li, Y., Liu, Y., Wang, Y., Zhang, Y., Huang, Y., Li, Y., Wu, Y., Liu, Y., Pan, Y., Zheng, Y., Hong, Y., Shi, Y., Feng, Y., Jiang, Z., Han, Z., Wu, Z.-F., and Liu, Z. Wan: Open and advanced large-scale video generative models. *arXiv preprint arXiv:2503.20314*, 2025.

Wang, J., Ma, Y., Guo, J., Xiao, Y., Huang, G., and Li, X. Cove: Unleashing the diffusion feature correspondence for consistent video editing. *Advances in Neural Information Processing Systems*, 37:96541–96565, 2024a.

Wang, J., Pu, J., Qi, Z., Guo, J., Ma, Y., Huang, N., Chen, Y., Li, X., and Shan, Y. Taming rectified flow for inversion and editing. *arXiv preprint arXiv:2411.04746*, 2024b.

Wang, J., Pu, Y., Han, Y., Guo, J., Wang, Y., Li, X., and Huang, G. Gra: Detecting oriented objects through group-wise rotating and attention. In *European Conference on Computer Vision*, pp. 298–315. Springer, 2024c.

Wei, Y., Zhang, S., Yuan, H., Han, Y., Chen, Z., Wang, J., Zou, D., Liu, X., Zhang, Y., Liu, Y., et al. Routing matters in moe: Scaling diffusion transformers with explicit routing guidance. *arXiv preprint arXiv:2510.24711*, 2025.

Wimbauer, F., Wu, B., Schoenfeld, E., Dai, X., Hou, J., He, Z., Sanakoyeu, A., Zhang, P., Tsai, S., Kohler, J., et al. Cache me if you can: Accelerating diffusion models through block caching. pp. 6211–6220, 2024.

Wu, C., Li, J., Zhou, J., Lin, J., Gao, K., Yan, K., Yin, S.-m., Bai, S., Xu, X., Chen, Y., et al. Qwen-image technical report. *arXiv preprint arXiv:2508.02324*, 2025.

Xi, H., Yang, S., Zhao, Y., Xu, C., Li, M., Li, X., Lin, Y., Cai, H., Zhang, J., Li, D., et al. Sparse videogen: Accelerating video diffusion transformers with spatial-temporal sparsity. 2025.

Xiang, J., Lv, Z., Xu, S., Deng, Y., Wang, R., Zhang, B., Chen, D., Tong, X., and Yang, J. Structured 3d latents for scalable and versatile 3d generation. *arXiv preprint arXiv:2412.01506*, 2024.

Xue, L., Gao, M., Xing, C., Martín-Martín, R., Wu, J., Xiong, C., Xu, R., Niebles, J. C., and Savarese, S. Ulip: Learning a unified representation of language, images, and point clouds for 3d understanding. In *Proceedings of the IEEE/CVF conference on computer vision and pattern recognition*, pp. 1179–1189, 2023.

Yang, Z., Teng, J., Zheng, W., Ding, M., Huang, S., Xu, J., Yang, Y., Hong, W., Zhang, X., Feng, G., et al. Cogvideox: Text-to-video diffusion models with an expert transformer. *arXiv preprint arXiv:2408.06072*, 2024.

Zhang, J., Wei, J., Zhang, P., Zhu, J., and Chen, J. Sageattention: Accurate 8-bit attention for plug-and-play inference acceleration. 2025.

Zhao, W., Han, Y., Tang, J., Wang, K., Song, Y., Huang, G., Wang, F., and You, Y. Dynamic diffusion transformer. *arXiv preprint arXiv:2410.03456*, 2024.

Zhao, Z., Lai, Z., Lin, Q., Zhao, Y., Liu, H., Yang, S., Feng, Y., Yang, M., Zhang, S., Yang, X., et al. Hunyuan3d 2.0: Scaling diffusion models for high resolution textured 3d assets generation. *arXiv preprint arXiv:2501.12202*, 2025.

Zheng, K., Wang, Y., Ma, Q., Chen, H., Zhang, J., Balaji, Y., Chen, J., Liu, M.-Y., Zhu, J., and Zhang, Q. Large scale diffusion distillation via score-regularized continuous-time consistency. *arXiv preprint arXiv:2510.08431*, 2025a.

Zheng, Y., Ren, Y., Xia, X., Xiao, X., and Xie, X. Dense2moe: Restructuring diffusion transformer to moe for efficient text-to-image generation. In *Proceedings of*

the IEEE/CVF International Conference on Computer Vision, pp. 18661–18670, 2025b.

Zhou, J., Wang, J., Ma, B., Liu, Y.-S., Huang, T., and Wang, X. Uni3d: Exploring unified 3d representation at scale. *arXiv preprint arXiv:2310.06773*, 2023.